

Ultrasonic welding of thermoplastic composites

A comparison between polyetheretherketone and low-melt polyaryletherketone as resin in the adherends and energy directors

Brito, C. B.G.; Teuwen, J.; Dransfeld, C. A.; Villegas, I. F.

DOI

[10.1016/j.compositesb.2025.112264](https://doi.org/10.1016/j.compositesb.2025.112264)

Publication date

2025

Document Version

Final published version

Published in

Composites Part B: Engineering

Citation (APA)

Brito, C. B. G., Teuwen, J., Dransfeld, C. A., & Villegas, I. F. (2025). Ultrasonic welding of thermoplastic composites: A comparison between polyetheretherketone and low-melt polyaryletherketone as resin in the adherends and energy directors. *Composites Part B: Engineering*, 296, Article 112264. <https://doi.org/10.1016/j.compositesb.2025.112264>

Important note

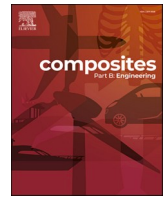
To cite this publication, please use the final published version (if applicable). Please check the document version above.

Copyright

Other than for strictly personal use, it is not permitted to download, forward or distribute the text or part of it, without the consent of the author(s) and/or copyright holder(s), unless the work is under an open content license such as Creative Commons.

Takedown policy

Please contact us and provide details if you believe this document breaches copyrights. We will remove access to the work immediately and investigate your claim.



Ultrasonic welding of thermoplastic composites: A comparison between polyetheretherketone and low-melt polyaryletherketone as resin in the adherends and energy directors

C.B.G. Brito ^{*}, J. Teuwen, C.A. Dransfeld, I.F. Villegas

Aerospace Structures and Materials Department, Faculty of Aerospace Engineering, Delft University of Technology, Kluyverweg 1, 2629 HS, Delft, the Netherlands

ARTICLE INFO

Handling Editor: Dr Uday Vaidya

ABSTRACT

Our aim with this work was to evaluate how the thermoplastic resin used in the composite adherends and on the energy director affected the static ultrasonic welding process in both parallel and misaligned configurations. Polyetheretherketone (PEEK) and low-melt polyaryletherketone (LMPAEK) were the resins used and their thermomechanical properties were characterized via dynamic-mechanical analysis and modulated differential scanning calorimetry. With parallel adherends, neither the welding time nor the through-thickness heating in the adherends vary significantly. This similarity was attributed to a larger heat capacity of the PEEK energy director counterbalancing its higher viscoelastic heating rate. With misaligned adherends, the welding time was larger for PEEK welds than for LMPAEK welds and LMPAEK adherends presented a larger through-thickness heating. These effects were attributed to the larger bulk viscoelastic heating rate of carbon fibre reinforced/LMPAEK adherends adding up to the lower heat capacity of LMPAEK.

1. Introduction

The aerospace industry has increased its use of thermoplastic composites in the last decades. This greater interest is a result of several appealing properties that thermoplastic resins present, such as high chemical and impact resistance, almost infinite shelf life and ease, cost-effective manufacturing via hot press forming, for example [1–4]. In addition to those, thermoplastics can also be remelted without losing their original mechanical properties, which also makes them recyclable and weldable [5–7], in contrast to thermoset resins. These advantages over thermosets derive from the difference in their chemical structures: thermosets present a cross-linked network while thermoplastic polymer chains are not cross-linked, which allows them to flow when heated up [8–10]. Hence, the recyclability and formability of thermoplastics allows for more sustainable end-of-life solutions, while its weldability opens up the possibility of a wide variety of fusion bonding techniques to be used.

Fusion bonding techniques, also known as *welding*, consist of locally heating up the polymer until a viscous state is reached. Through a process called *healing*, the interdiffusion of the polymer chains across the joining interface occurs until the joining interface completely disappears

and the mechanical strength of the welded area develops. Finally, the joint is consolidated by cooling down the polymer. The way that heat is generated at the weld interface is usually used to categorise the different welding techniques. Following this criteria, a welding technique can be categorised in: (1) thermal, when an external source heats up the materials to be welded, is then removed and the molten welded parts are brought together via a forging pressure (this category can also be found in literature as *Two-Stage*, since two separate stages are involved in the process – melting and forging); (2) electromagnetic, when a magnetic material is inserted at the weld interface which is heated via a magnetic field, melting the polymer in its surroundings; and (3) frictional, when the heat generation arises from frictional work at the weld interface under a certain pressure [7,11].

Examples of thermal welding are hot tool (plate), hot gas, infrared and laser welding. For electromagnetic welding, examples include induction, resistance, dielectric and microwave welding and for friction welding, spin, stir and ultrasonic welding. Each one of these welding techniques present advantages and disadvantages, depending on the shape of the parts to be welded, size, composite reinforcement type, optical and electrical properties and if the weld is between similar or dissimilar materials [2,7,9–16]. Specifically for high performance

* Corresponding author.

E-mail address: c.brito@tudelft.nl (C.B.G. Brito).

<https://doi.org/10.1016/j.compositesb.2025.112264>

Received 14 December 2024; Received in revised form 5 February 2025; Accepted 9 February 2025

Available online 10 February 2025

1359-8368/© 2025 The Authors. Published by Elsevier Ltd. This is an open access article under the CC BY-NC license (<http://creativecommons.org/licenses/by-nc/4.0/>).

composites made with continuous fibre reinforcement, resistance, induction and ultrasonic welding are generally considered the most suitable techniques [11,17–19]. In resistance welding, a conductive element is placed at the weld interface. Current is then applied to this conductive element which, according to Joule's Law, will generate heat, which in turn heats up the polymer material on its surroundings. Despite of its simplicity, the main drawbacks for resistance welding are the permanent presence of a foreign material at the weld interface, the possibility of fibre movement, and uneven heating [18–20]. Induction welding, on the other hand, induces eddy currents on an electrically conductive and magnetically susceptible material at the vicinity of an alternating electromagnetic field. The material then heats up via Joule losses, dielectric heating and magnetic hysteresis. Although the need of a foreign material can be overcome in the case when carbon fibres are used as reinforcement due to their conductive nature, bulk heating, heating uniformity, and absence of feedback during the welding process have been reported as the main challenges of this technique [17,19,21,22].

Finally, ultrasonic welding uses a metal horn (sonotrode) to apply a constant force in combination to high-frequency and low-amplitude mechanical vibrations on top of the parts to be welded [23]. Besides its high energy efficiency, fast processing times, possibility for in-situ monitoring and for welding of dissimilar materials [1,23–25], another advantage of ultrasonic welding is that heat generation is focused at the weld interface by the use of a resin-rich element called *energy director*. Therefore, a foreign material is not required at the weld interface such as other welding techniques like resistance welding [17,26]. The difference in the elastic modulus of the energy director in comparison to the composite adherends is what promotes higher cyclic strain at the weld interface. The higher cyclic strain results in frictional and viscoelastic heating to mainly occur at the weld interface, generating the heat that will melt the energy director during the vibration phase of the process. Once the material is molten, the static force applied by the sonotrode squeezes the molten material out, further promoting intimate contact between the adherends surfaces, with the bond being established by the molecular inter-diffusion of the adherends polymer chains through the weld interface [26].

Several studies have been devoted to deeply understand the ultrasonic welding process, such as studying its heating and vibrating mechanisms [27,28] and numerically modelling them [29], contributing to its upscaling and industrialization. For instance, one of our previous works investigated how ultrasonic welding is affected by the lack of parallelism between the welded parts [30], which is a scenario that the process may face when used in a manufacturing line. Another work investigated mitigation approaches to overcome or diminish the effects caused by the lack of parallelism between the welded parts [31]. Other studies focused on the transition from a static process (i.e. the welded area has the same size of the sonotrode imprint) to a continuous process (i.e. the welded area is longer than the sonotrode imprint) [32]. In the continuous process, longer seams are obtained because the sonotrode moves along the welded parts. Therefore, understanding the differences that this translational movement of the sonotrode brings in is an essential step towards the upscaling and commercialization of ultrasonic welding [33,34].

In all of these works, different thermoplastic resins have been used to produce the welded parts and energy director: poly(methyl methacrylate) (PMMA) [27], polyetherimide (PEI) [24,28,29], polyetheretherketone (PEEK) [30,31] and polyphenylene sulphide (PPS) [32–34]. Although they are all thermoplastic resins, many properties differ from one to the other. PMMA has great optical properties and low specific weight, making it perfect for aircraft windows [35,36]. PEI is mostly used in aircraft interior applications due to its low resistance to fuel and synthetic hydraulic oil [37]. PPS, although in the same price range of PEI, is a more resistant resin (higher thermal stability, chemical resistance and flame retardancy) and is therefore used in a wider variety of aircraft parts [35,38]. PEEK is the most preferred one for primary aircraft structures due to its superior mechanical properties and

chemical resistance. However, its high melting point imposes a challenge to its manufacturing, making it one of the most expensive thermoplastic materials [37,39]. Low-melt polyaryletherketone (LMPAEK) has then been developed as an alternative to PEEK, since it promises to keep PEEK's mechanical properties and glass transition temperature while only reducing its melting point [39,40]. Such differences can potentially affect the ultrasonic welding process. For example, the heating mechanisms involved in ultrasonic welding (frictional and viscoelastic) are highly dependent on the material glass transition temperature (T_g) [24]. Therefore, the fact that the T_g can greatly vary when changing the resin used in the adherends and energy director (from 97 °C for PPS [41] to around 220 °C for PEI [25]) can result in different welding times. Similarly, the storage and loss moduli of the resin affect the amount and rate of viscoelastic heat generated during the ultrasonic welding process [24,26], potentially resulting in differences in the temperature evolution at the weld interface and in the welding time. When misaligned adherends are being investigated, the temperature evolution and heat generated during the process are even more crucial for the quality of the final weld, since it will affect the through-thickness heating and squeeze flow of the molten material [30,31]. Up to now, no studies that evaluate how the ultrasonic welding process is affected depending on the resin used to manufacture the adherends and the energy director were found. This knowledge gap is an issue for both academia and industry. For the former, it hinders the comparison between studies that use different materials, while it contributes to making the aviation industry dependent on few specific resins, since change can lead to unexpected and unknown results.

In this work, our aim is to investigate how the resin used as matrix in the adherends and in the energy director affects the ultrasonic welding process of welds made with both parallel and misaligned adherends and other side-effects such as the through-thickness heating on the adherends. The resins used in this study were polyetheretherketone (PEEK) and low-melt polyaryletherketone (LMPAEK). PEEK was chosen due to its preferred properties for aerospace applications and to allow a direct comparison with previous works [30,31], while LMPAEK was chosen as the new state of the art resin system for aerospace structures since it has a lower processing temperature than PEEK while keeping a similar chemical backbone. Power and displacement curves and temperature measurements were used to assess the effects on the ultrasonic welding process. Cross-sectional micrographs were used to assess the through-thickness heating on the welds and analysis of fracture surfaces was used to get further insight on the crystallinity of each resin. Dynamic-mechanical analysis (DMA) and modulated differential scanning calorimetry (mDSC) were used to characterize the thermo-mechanical properties of the two resins, since it is expected that differences could affect the viscoelastic heating rate and temperature increase during the ultrasonic welding process.

2. Methodology

2.1. Materials

Polyetheretherketone (PEEK) and low-melt polyaryletherketone (LMPAEK) reinforced with carbon 5-harness satin woven from Toray Advanced Composites (the Netherlands) were used to produce the specimens used in this paper. Nominal fibre volume content of the prepregs was 58 % and 57 % for PEEK and LMPAEK, respectively, and the type of the carbon fibre was T300JB for both prepregs. Nominal glass transition temperature (T_g) was approximately 145 °C for both materials but melting temperature (T_m) differed, being 343 °C for PEEK and 305 °C for LMPAEK [42,43]. The stacking sequence of the laminates was [(0/90)₃]_s, which were consolidated in a hot platen press at 385 °C and 10 bar for 30 min for C/PEEK or at 365 °C and 10 bar for 30 min for C/LMPAEK. The nominal thickness of the consolidated laminate was 1.90 mm for C/PEEK and 1.80 mm for C/LMPAEK. Adherends measuring 25.4 mm by 101.6 mm were cut out of the laminates with a

water-cooled diamond blade with the main apparent orientation of the fibres parallel to their longer side.

For the PEEK energy director (ED), a 0.25 mm-thick flat film of VICTREX® APTIV® 1000 PEEK resin supplied by Goodfellow Cambridge Ltd (England) was used. For the LMPAEEK ED, a 0.20 mm- and a 0.06 mm-thick flat film of APTIV AE™ LMPAEEK resin provided by VICTREX® (United Kingdom) were placed between two stainless steel plates and consolidated together in a hot platen press at 300 °C and 20 bar for 35 min, resulting in film with a final nominal thickness of approximately 0.25 mm. Note that to avoid unwanted flow of the resin, the LMPAEEK ED was consolidated at a temperature just below the melting temperature of LMPAEEK.

2.2. Ultrasonic welding process

Two types of welds were produced in this work: C/PEEK adherends welded using PEEK ED and C/LMPAEEK adherends welded using LMPAEEK ED. They will be referred to as *PEEK welds* and *LMPAEEK welds*, respectively from now on. The adherends were welded in a single-lap configuration (overlap of 12.7 mm length and 25.4 mm width) with a 20 kHz ultrasonic welding machine (HiQ DIALOG SpeedControl) from Herrmann Ultraschall, Germany. A rectangular sonotrode with a contact area of 15 mm by 30 mm was used. For the amplitude of vibration and welding force, a variety of combinations can deliver similar high-strength welded joints [24,44]. Similarly, different combinations of consolidation force and time can affect the final quality of the welded joints [34]. Based on previous works [24,30,31,45,46], the peak-to-peak amplitude of vibration was set as 86.2 μm with a welding force of 500 N, consolidated with a consolidation force of 500 N applied for 4s for all cases. The process was displacement-controlled, i.e., the vibration stopped when the downward vertical displacement of the sonotrode, d_0 , reached a set value. Two values for d_0 were used in this work: 0.25 mm and 0.03 mm. The value of 0.25 mm, equal to the thickness of the EDs, was used to obtain *full* welds with complete power curves and temperature measurements at the weld interface. The value of 0.03 mm was used when our interest was at the *onset* of the downward movement of the sonotrode: the moment when the molten material within the overlap area starts to be squeezed out. Up to the onset of the downward movement of the sonotrode is when most of the heating mechanisms (frictional and viscoelastic heating) responsible to take the materials to their melting point take place [24,26] and a relatively thick resin layer is still present at the weld interface [24]. Using the onset of the downward movement of the sonotrode allows a more consistent comparison between different cases without the need to optimize the parameters to obtain optimum welds. We refer to optimum welds as those that yield the highest weld strength, usually associated with a complete welded

overlap area and minimum fibre deformation [24,44]. Optimum welds are obtained by stopping the welding process at the so called *optimum displacement* (when the process is displacement-controlled), which is dependent on the setup, welding parameters, materials and ED geometry [32,44–48]. Since our goal is to understand how the resin affects the main heating mechanisms involved in the ultrasonic welding process, we focused on the onset of the downward movement of the sonotrode.

The jig used to hold the adherends in place is shown in Fig. 1a and it consists of two metal bars used to clamp each adherend to the base of the anvil. In our previous work [30], we showed that the misalignment between the adherends and the compliance of the top adherend is affected by the distance between the sonotrode and the clamp holding the top adherend. Shorter clamping distances for the top adherend (e.g., 5 mm) were found to increase the angle between adherends and to decrease the compliance of the top adherend, making the welding process more challenging [30]. To evaluate the effect of using different resins on the ultrasonic welding process in varied scenarios, adherends were welded in *parallel* (ideal) and *misaligned* configurations (Fig. 1b and 1c show a schematic of each configuration). For the parallel configuration, the clamping distance of the top clamp was kept at 50 mm, which is the largest one allowed by the setup. For the misaligned configuration, this distance was kept at 5 mm, being the shortest one while ensuring that the sonotrode would not touch the metal bar. The distance between the sonotrode and the clamp holding the bottom adherend was kept at 25 mm for all cases. A supporting base is usually used under the top adherend to ensure parallelism between the adherends (see Fig. 1). For the parallel configuration, a supporting base thickness of 1.90 mm for C/PEEK adherends and of 1.80 mm for C/LMPAEEK adherends were used, while the thickness of the supporting base was 1.50 mm to keep a misalignment angle of approximately 2.70° for the misaligned configuration. We decided to use a more conservative misalignment angle than in our previous work [31] because we believe that comparison and evaluation of the through-thickness heating between the adherends made with different resins would be rather difficult if we were working with the most severe angle effects (largest through-thickness heating and longest welding time). Table 1 shows a summary of all the welding and clamping parameters used in this study and includes a list of the characterisation methods for each configuration.

2.3. Temperature measurements

To measure the temperature evolution at the weld interface for PEEK and LMPAEEK welds, two K-type thermocouples with a wire diameter of 0.1 mm were used, each one placed at longitudinally opposite edges of the overlap. These edges are called *Edge 1* (E1) and *Edge 2* (E2), according to Fig. 2. For misaligned welds, E1 corresponds to the free edge,

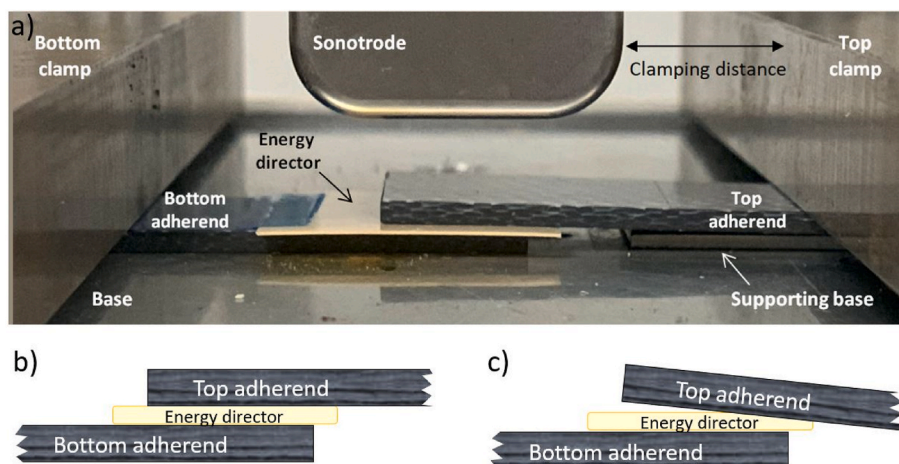


Fig. 1. a) Static ultrasonic welding process setup with schematics of b) parallel and c) misaligned configurations.

Table 1

Summary of the parameters used for different tests. All tests were consolidated with a consolidation force of 500 N for 4 s.

Case	Composite Matrix/ED resin	Clamping distance [mm]	Base thickness [mm]	Study	d_0 [mm]	Number of samples
Parallel	PEEK	50	1.90	• Temperature measurements	0.25	At least 3
				• Cross-sectional micrographs	0.03	1
	LMPAEK	50	1.80	• Temperature measurements	0.25	At least 3
Misaligned	PEEK	5	1.50	• Cross-sectional micrographs	0.03	1
				• SEM images	0.03	1
	LMPAEK	5	1.50	• Temperature measurements	0.25	At least 3
				• Cross-sectional micrographs	0.03	1
				• Temperature measurements	0.25	At least 3
• Cross-sectional micrographs	0.03	1				

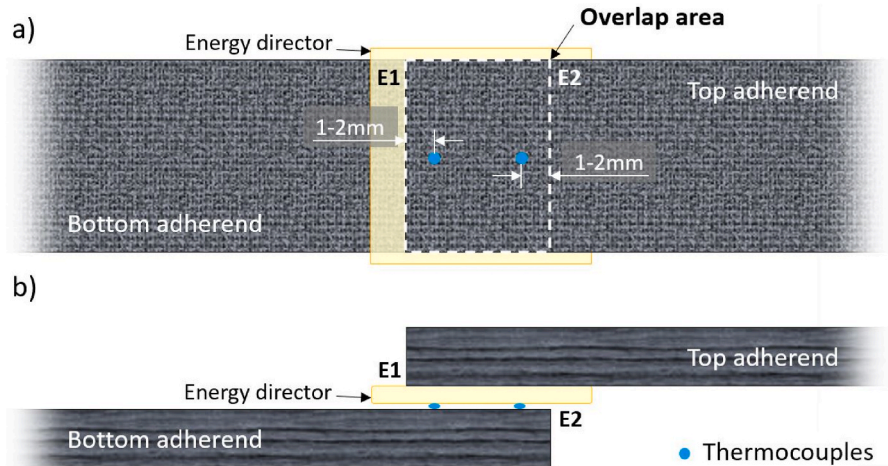


Fig. 2. a) Top-view and b) side-view schematics of the position of the thermocouples for temperature measurements. The thermocouples were placed 1–2 mm away from the transversal edges of the overlap (E1 and E2).

while E2 corresponds to the compressed edge. Once the bottom adherend was clamped to the base of the jig, the thermocouples were placed on its top surface, 1–2 mm away from E1 and E2, within the overlap, on the longitudinal midline of the adherends. Adhesive tapes placed outside the overlap were used to secure the thermocouples in place. Once the thermocouples were correctly positioned on the surface of the bottom adherend, the energy director was stacked on top of them, followed by the top adherend. The temperature sampling rate was 1 kHz.

2.4. Physical characterisation

Dynamic Mechanical Analysis (DMA) was used to compare the glass transition temperature and the evolution of the storage and loss moduli of EDs made with PEEK and LMPAEK and C/PEEK and C/LMPAEK adherends and the tests were performed on a RSA-G2 Solids Analyzer from TA Instruments. For the EDs, a tensile setup was used from 25 °C to 250 °C with a heating rate of 3 °C/min and a frequency of 1Hz. For each resin, two samples of 10 mm × 25 mm were cut from the same 0.25 mm-thick films used to manufacture the EDs and tested. For the adherends, a 3-point bending setup was used from 25 °C to 250 °C with a heating rate of 2 °C/min and a frequency of 1Hz. For each resin, at least two samples of 12 mm × 40 mm were cut from the same laminates used to manufacture the adherends. The glass transition temperature was then determined as being the temperature where the peak in loss modulus occurred.

Modulated Differential Scanning Calorimetry (mDSC) was used to obtain the evolution of the heat capacity of both resins up to their respective melting point and to estimate the melting enthalpy of each resin. For that, a DSC250 from TA Instruments was used for PEEK and LMPAEK EDs. Two samples for each resin were tested, weighing 6.5 ± 0.5 mg for PEEK and 6.9 ± 0.1 mg for LMPAEK. A modulation amplitude

of 1 °C and a modulation period of 100s were used in a temperature range from 25 °C to 400 °C for PEEK and to 350 °C for LMPAEK.

2.5. Microscopy analysis

To analyse the through-thickness heating on consolidated welds, cross-sectional microscopy was performed on samples cut along the longitudinal direction of the welds, at the centre of the adherends width. The welds were stopped at the onset of the downward movement ($d_0 = 0.3$ mm) of the sonotrode to keep repeatability and comparability between the two weld types and consolidation force was applied at the end so the effect of the squeeze flow could also be assessed. The samples were embedded in epoxy resin and polished with a Struers Tegramin-20 polisher. The cross-sections were then analysed with a Keyence VH-Z100UR digital microscope. The cross-section micrographs of the parallel case are also used to access the adherends manufacturing process quality, given that the heat affected zone in the parallel configuration is known to be limited to the layers closer to the weld interface [46].

To analyse the weld interface, scanning electron microscopy (SEM) was performed on fracture surfaces obtained from single lap shear testing and a JEOL JSM-IT100 Scanning Electron Microscope was used. Single lap shear testing was conducted in a Zwick/Roell 250 kN universal testing machine with a crosshead speed of 1.3 mm/min on samples with parallel adherends (as can be seen in Table 1). The single lap shear tests were performed to expose the weld interfaces. As the welds were stopped at the onset of the downward movement of the sonotrode ($d_0 = 0.3$ mm) to study flow, their strength is not representative of the highest strength [24,44]. Therefore, the mechanical results from the single lap shear test are not included in this work.

3. Results

3.1. Ultrasonic welding: parallel configuration

Fig. 3 shows the power and displacement curves of full welds as well as the associated temperature measurements at the weld interface for the parallel configuration. Here we chose to show the temperatures at only E1 because thermocouples at E2 were more susceptible to failure during the ultrasonic welding process and because the difference in temperature between the two edges, which occurs due to a higher pressure being applied on E2, is not significant enough to affect the process time on parallel configurations [30]. From Fig. 3a, no difference in the duration of the welding process between PEEK and LMPAEK welds

is observed. There are no significant differences in power peak or time at which the power peak occurs for the PEEK and LMPAEK welds. According to the temperature profiles showed in Fig. 3b, welds made with either resin reach their respective melting temperature very early in the process. The temperature profile of LMPAEK welds only starts to diverge from the ones of PEEK closer to the onset of the downward movement of the sonotrode, after which LMPAEK welds reach higher temperatures than PEEK welds.

Fig. 4 shows the cross-sectional micrographs of consolidated PEEK and LMPAEK parallel welds stopped at the onset of the downward movement of the sonotrode. As can be seen in this Figure, the matrix only experiences a change in colour (or shade of grey) at and in the vicinity of the weld interface, as indicated by the black and red arrows.

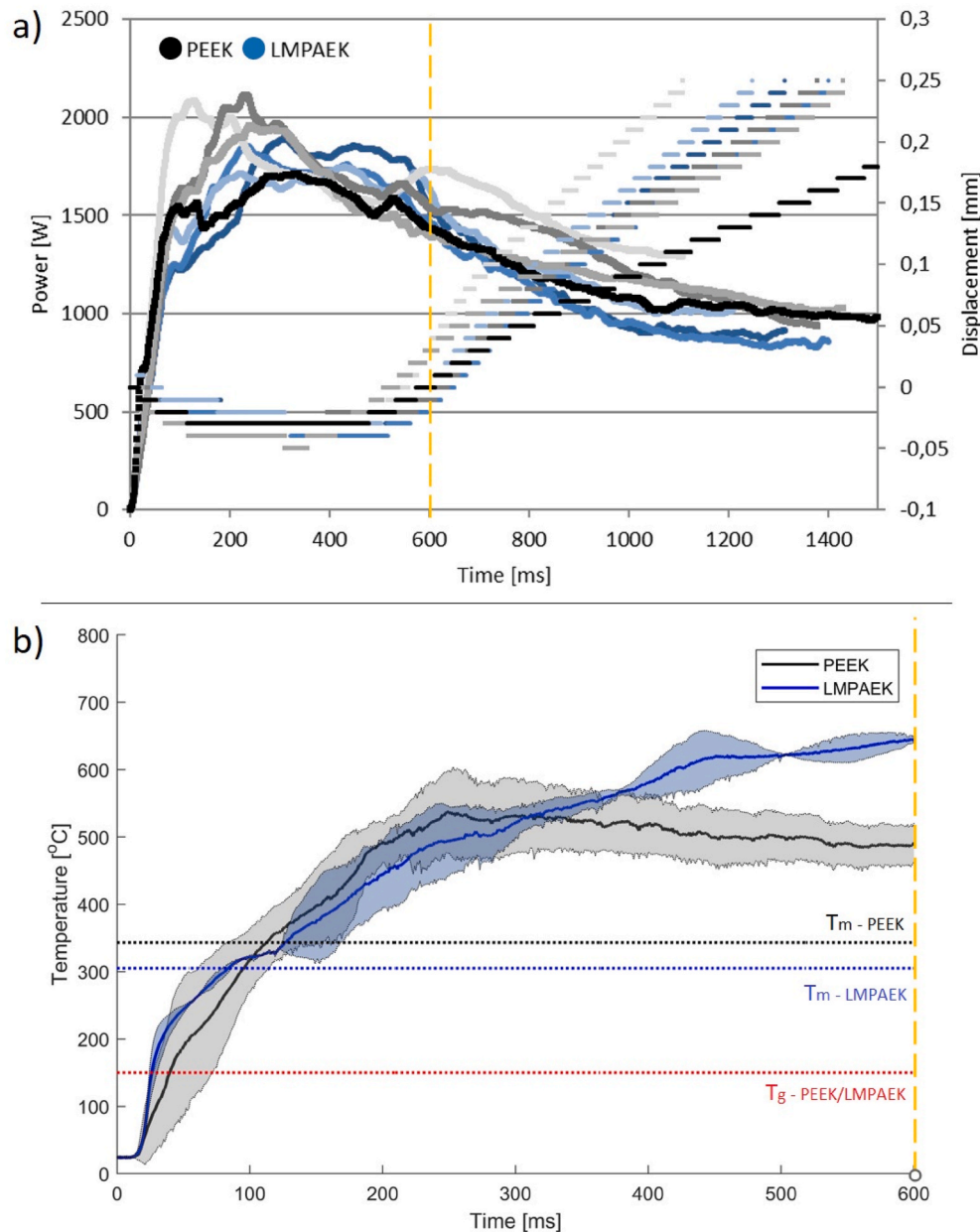


Fig. 3. a) Power curves (solid lines) and displacement curves (dashed lines) and b) temperature evolution at the interface between bottom adherend and ED for PEEK and LMPAEK parallel welds up until the onset of flow. Solid black and blue lines indicate the average of at least three temperature measurements. The shadowed regions indicate the standard deviation of the measurements. The red dotted line at 150 °C indicates the nominal glass transition temperature of PEEK and LMPAEK, the blue dotted line at 300 °C indicates the melting temperature of LMPAEK and the black dotted line at 340 °C indicates the melting temperature of PEEK. The vertical yellow dashed line indicates when the onset of the downward movement of the sonotrode occurs. (For interpretation of the references to colour in this figure legend, the reader is referred to the Web version of this article.)

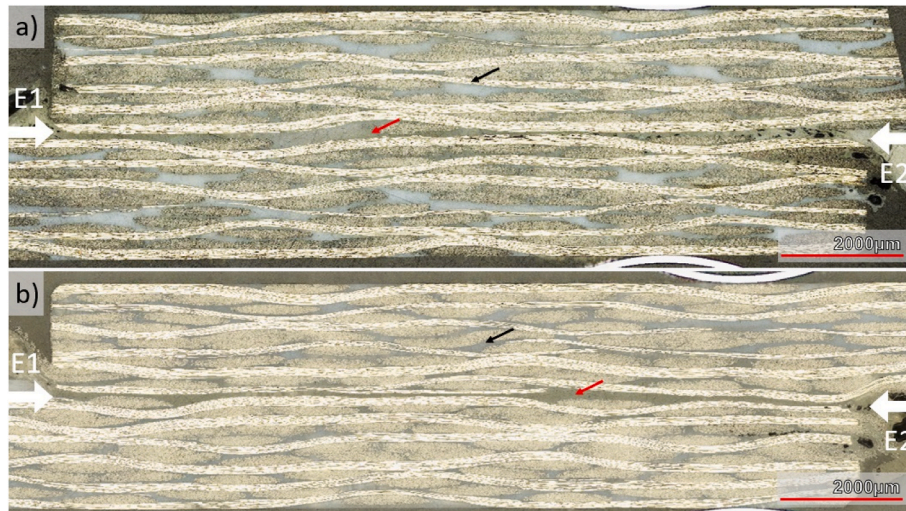


Fig. 4. Cross-section in the longitudinal direction of parallel welds made with a) PEEK and b) LMPAEK stopped at the onset of the downward movement of the sonotrode (displacement = 0.03 mm). Consolidation force of 500 N was applied for 4 s. Black and red arrows indicate different shades of grey observed in the resin-rich areas in the adherends. (For interpretation of the references to colour in this figure legend, the reader is referred to the Web version of this article.)

No porosity is observed at the layers farther from the weld interface.

3.2. Ultrasonic welding: misaligned configuration

Fig. 5 shows the power and displacement curves for PEEK and LMPAEK welds made with misaligned adherends. A clear difference can be seen in the duration of the process, with LMPAEK welds finishing in almost half of the time required for PEEK welds. Regarding the power consumed during the process, the resin type does not seem to significantly affect the power curves until around 2000 ms, time from which LMPAEK welds present a considerably faster increase in power than PEEK welds. Such increase in power is related to the downward movement of the sonotrode and consequent squeeze out of molten material.

Fig. 6 shows the temperature evolution at E1 and E2 over time for PEEK and LMPAEK welds, until the onset of the downward movement of the sonotrode. For both resins, the onset of the movement starts when the temperature at E2 gets closer to the melting temperature of the

resins. However, LMPAEK welds reach LMPAEK T_m earlier than PEEK welds reach PEEK T_m and present an overall higher temperature profile than PEEK welds, with a rate of change in temperature approximately 1.7 times higher than the one of PEEK (0.104 °C/ms and 0.061 °C/ms, respectively). These rates of change in temperature were calculated by taking the delta in temperature between each resin T_m (approximately at 340 °C for PEEK and 300 °C for LMPAEK) and the temperature at which the downward movement of the sonotrode occurs (which is at approximately 650 °C for both resins) and dividing it by the corresponding time period in which the delta in temperature occurred. Therefore, a delta in temperature of 310 °C for PEEK and of 350 °C for LMPAEK was divided per 5100 ms for PEEK and per 3350 ms for LMPAEK, respectively.

Fig. 7 shows the cross-sectional micrographs of consolidated PEEK and LMPAEK welds stopped at the onset of the downward movement of the sonotrode. At E1, it is possible to observe that the composite layers of the C/LMPAEK top adherend are closer to each other than the composite layers of the C/PEEK top adherend at the same edge. Still close to E1, one

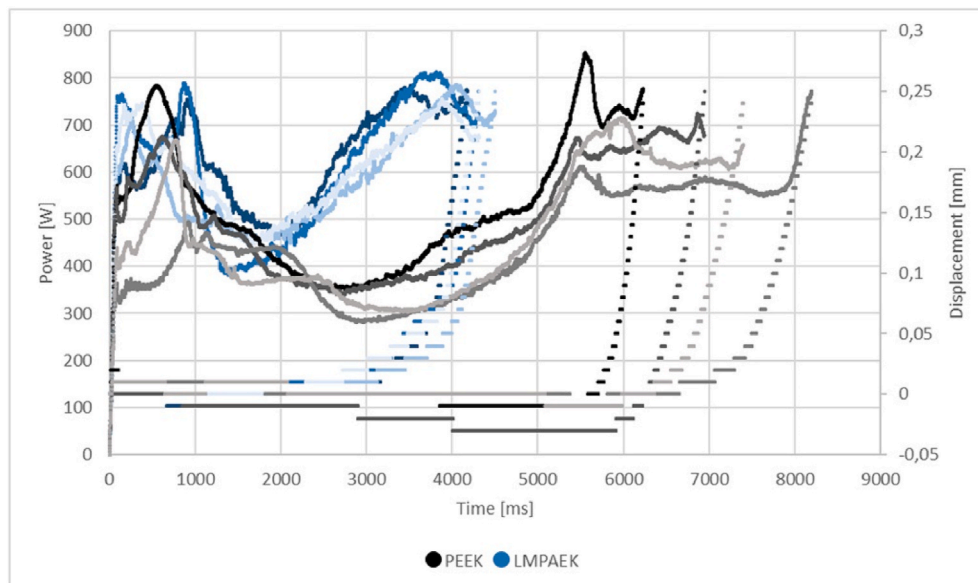


Fig. 5. Power curves (solid lines) and displacement curves (dashed lines) of misaligned cases for PEEK and LMPAEK. Different shades of grey and blue represent different samples. (For interpretation of the references to colour in this figure legend, the reader is referred to the Web version of this article.)

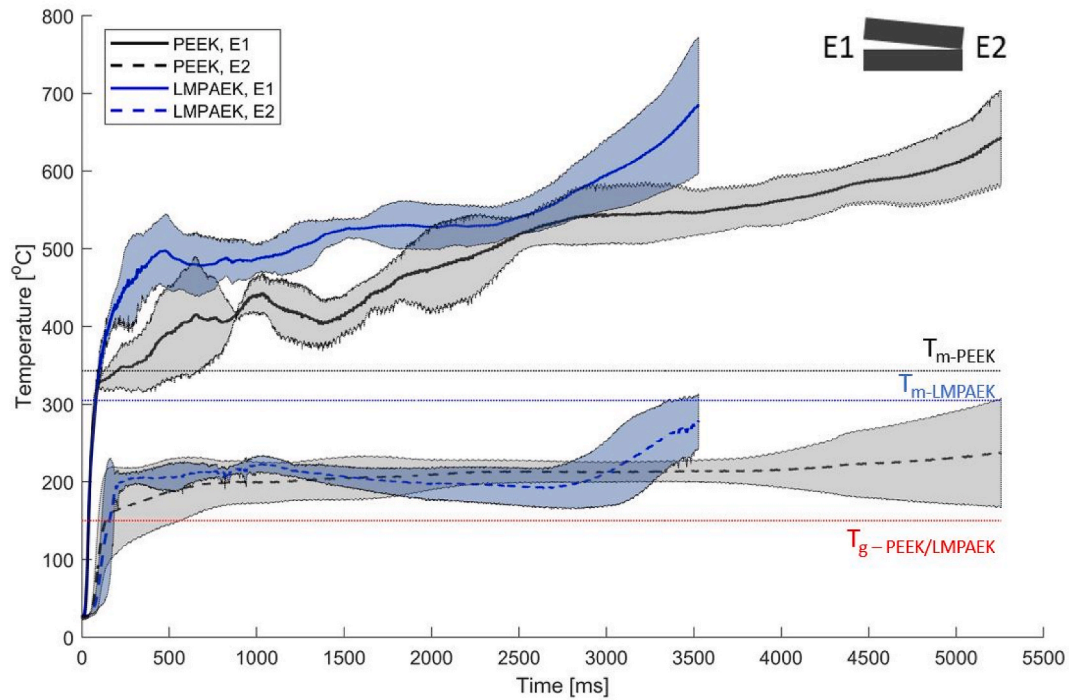


Fig. 6. Temperature evolution over time for PEEK and LMPAEK misaligned welds until the onset of the downward movement of the sonotrode. Black and blue lines (both solid and dashed) indicate the average of at least three temperature measurements. The shadowed regions indicate the standard deviation of the measurements. The red dotted line at 150 °C indicates the nominal glass transition temperature of PEEK and LMPAEK, the blue dotted line at 300 °C indicates the melting temperature of LMPAEK and the black dotted line at 340 °C indicates the melting temperature of PEEK. (For interpretation of the references to colour in this figure legend, the reader is referred to the Web version of this article.)

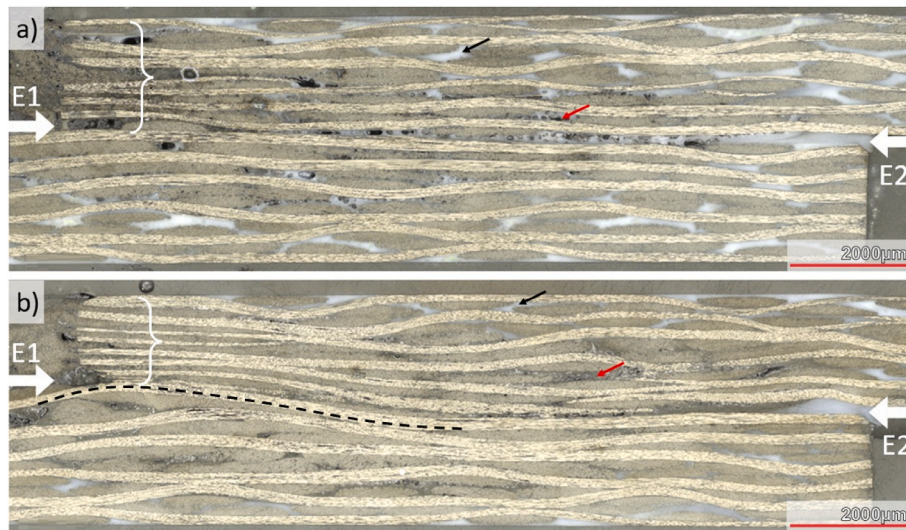


Fig. 7. Cross-section in the longitudinal direction of misaligned welds made with a) PEEK and b) LMPAEK. The welds were stopped at the onset of the downward movement of the sonotrode (displacement = 0.03 mm) and consolidation force of 500 N was applied for 4 s. The brackets indicate the difference in the concentration of layers in the top adherends at Edge 1. The white arrows indicate the position of the weld line. Black and red arrows indicate different shades of grey observed in the resin-rich areas in the adherends. (For interpretation of the references to colour in this figure legend, the reader is referred to the Web version of this article.)

can see that the layers of the C/PEEK bottom adherend are more parallel to each other than the layers of the C/LMPAEK bottom adherend, which presents a significant distortion, as indicated by the dashed black line. The voids observed within the C/PEEK adherends are larger in size and easier to identify than the ones present in the C/LMPAEK adherends. Finally, white (resin-rich) areas spread within the adherends layers are more present in C/PEEK than in C/LMPAEK adherends. For C/PEEK, these areas are clearly seen from the third to the sixth layers of both

adherends, along most of the overlap length. Contrarily, they are only seen towards the most outwards layers of the C/LMPAEK adherends.

3.3. Thermomechanical characterization

3.3.1. Energy directors

Fig. 8 shows the temperature dependency of the storage and loss moduli (E' and E'' , respectively) in tension mode of PEEK and LMPAEK

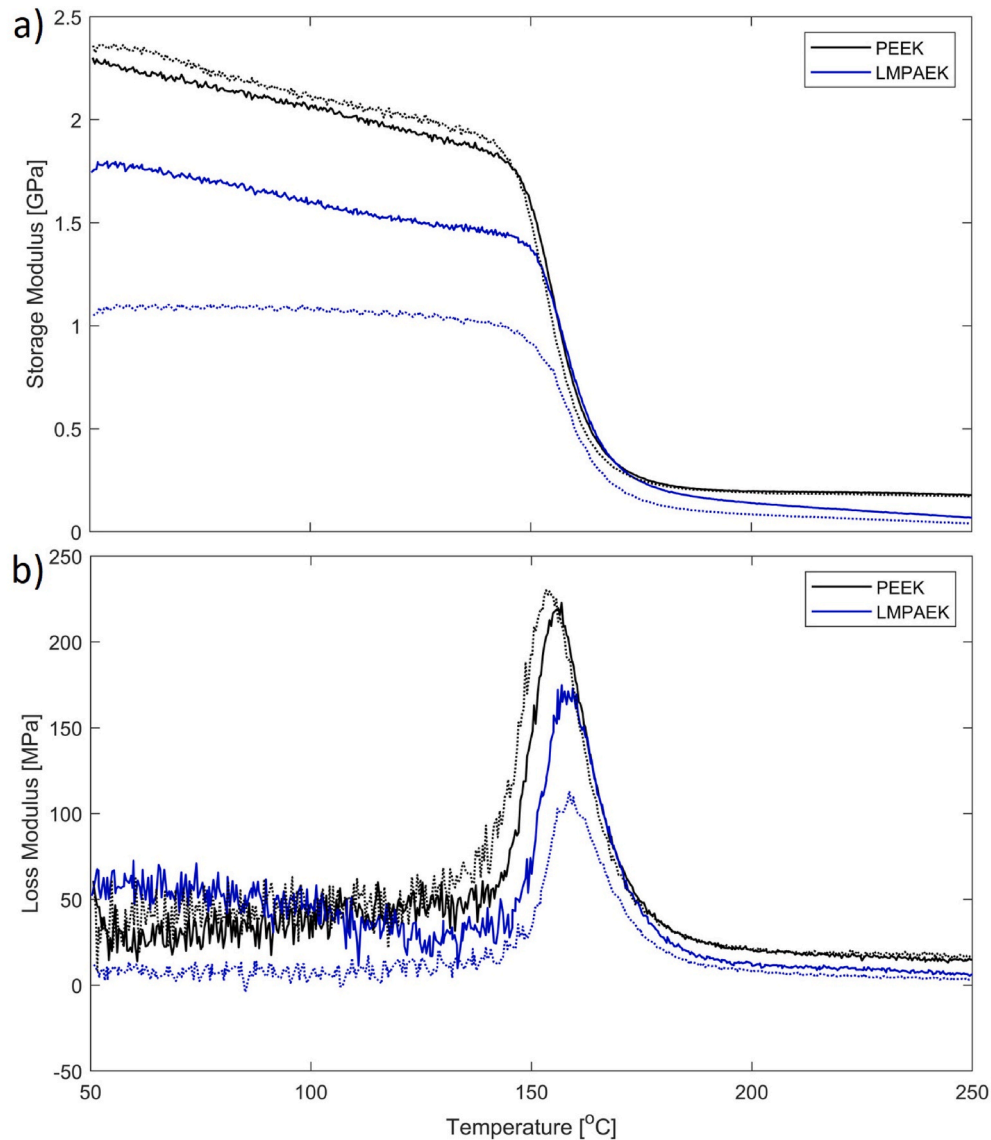


Fig. 8. Temperature dependency of a) Storage and b) Loss moduli of PEEK and LMPAEK EDs. Solid and dotted lines of same colour indicate duplicate tests. (For interpretation of the references to colour in this figure legend, the reader is referred to the Web version of this article.)

EDs obtained from DMA tests. An evident drop on the storage modulus is associated to the temperature at which the glass transition occurs. This drop occurs right after 150 °C for both PEEK and LMPAEK, indicating that both resins present a similar glass transition temperature. A similar interpretation can be done for the temperature at which the peak in the loss modulus occurs. As expected, the peak is observed on the loss modulus around the same temperature for both resins (156 °C). Overall, LMPAEK presents a lower storage modulus (between 23 % and 49 % lower) and a lower loss modulus peak at the T_g (between 22 % and 50 % lower) compared to PEEK.

Fig. 9 shows the thermal evolution of the heat capacity of PEEK and LMPAEK EDs obtained from mDSC tests. LMPAEK presents an overall slightly lower heat capacity than PEEK along the entire temperature range. This difference becomes significant when comparing the heat capacity of each resin at their corresponding melting temperatures (around 340 °C for PEEK and 300 °C for LMPAEK), where PEEK presents a heat capacity of approximate twice the one for LMPAEK. From the mDSC, the melting enthalpy was obtained by integrating the area under the melting peak for each of the resins, resulting in approximately 41 J/g for PEEK and 26 J/g for LMPAEK.

3.3.2. Adherends

Fig. 10 shows the temperature dependency of E' and E'' in bending mode of C/PEEK and C/LMPAEK adherends obtained from DMA tests. The overall storage modulus and the peak in the loss modulus are higher for C/LMPAEK adherends than for C/PEEK adherends (storage modulus of C/PEEK adherends is around 56 % and 44 % lower than C/LMPAEK adherends while loss modulus is around 15 % and 34 % lower) and a slight shift in the T_g occurs between the two types of adherends (from around 146 °C for C/PEEK adherends to around 158 °C for C/LMPAEK adherends).

4. Discussion

To assess how changing the resin type from PEEK to LMPAEK in the adherends and the ED affects the ultrasonic welding process, the power and displacement curves obtained as output from the welder equipment were used (Fig. 3a and Fig. 5). More specifically, we will focus on the time to reach the onset of the downward movement of the sonotrode since that is when most of the heating mechanisms responsible to take the materials to their melting point (frictional and viscoelastic heating) occur, as previously mentioned. Specifically to parallel cases, the onset

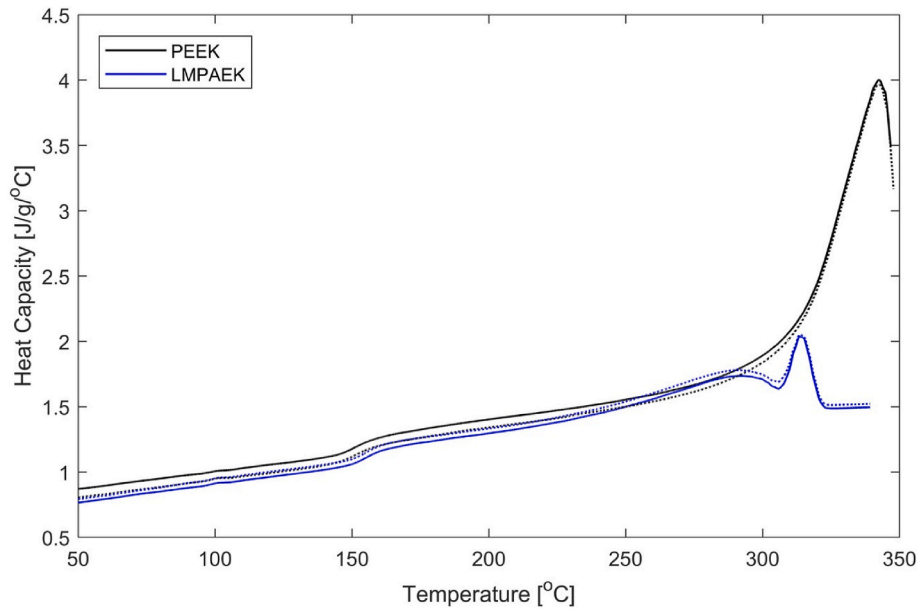


Fig. 9. Thermal evolution of heat capacity by mDSC. Solid and dotted lines of same colour indicate duplicate tests. (For interpretation of the references to colour in this figure legend, the reader is referred to the Web version of this article.)

of the downward movement of the sonotrode is usually called “onset of flow” since it is related to the moment when the energy director is completely molten and starts to be squeezed out of the welding area by the sonotrode [24]. To investigate the effects on the through-thickness heating of the adherends, cross-sectional micrographs were used.

For parallel adherends, the time until the onset of flow for the welds made with each resin was very similar (see Fig. 3a), with both cases reaching their corresponding T_m very early in the process (Fig. 3b). Only closer to the onset of the flow, a higher heating rate is observed for LMPAEK welds in comparison to PEEK welds, which seems to show a slight reduction in temperature increase. The cross-sectional micrographs (Fig. 4) indicate that no significant difference can be pointed out between PEEK and LMPAEK welds for the parallel configuration.

To understand the complex material interactions at the start of the heating phase and which material parameters play a significant role, a simple analytical calculation of the viscoelastic heating rate, \dot{Q}_{visc} , can help us for the parallel configuration. The viscoelastic heating rate can be estimated according to:

$$\dot{Q}_{visc} = \frac{\omega E_{ED}^* \varepsilon_{ED}^2}{2} \quad (1)$$

where ω is the frequency of vibration (20 kHz), E_{ED}^* is the loss modulus of the ED material and ε_{ED} is the cyclic strain on the ED. In turn, to estimate the cyclic strain on the ED, we assume that the welding stack adherend-ED-adherend can be modelled as an association of springs in series [49]. Hence, ε_{ED} can be estimated according to:

$$\varepsilon_{ED} = \frac{\Delta L}{\left[2 \frac{E_{ED}^* L_{Ad}}{E_{Ad}} + L_{ED} \right]} \quad (2)$$

where E is the transverse storage modulus of the element (either the ED (subscript ED) or the adherends (subscript Ad)), L is the element thickness and ΔL is the total deformation on the welding stack (hence half-peak of the amplitude of vibration, 43.1 μm).

We do not make use of the storage modulus presented in Fig. 10b because the DMA test for the adherends was performed in a 3-point bending setup. This setup would result in a high influence of the stiffness of the fibres in our results, which would not be realistic for the transverse storage modulus, mainly governed by the matrix properties.

Hence, we believe that the transverse storage modulus derived using the rule of mixtures proposed by Jacquet et al. [50] would deliver a better approximation. The composite is assumed to be isotropic [29]. The storage modulus of the carbon fibres is assumed as 180 GPa [29], while the storage modulus of the resins at room temperature are taken from the DMA results presented in Fig. 8 (2.30 GPa for PEEK and 1.40 GPa for LMPAEK). From the manufacturer, the fibre volume fraction is 58 % for PEEK and 57 % for LMPAEK [42,43]. However, when analysing the thickness of the laminates, the C/LMPAEK laminate was about 0.1 mm thinner than the C/PEEK laminate (1.8 mm versus 1.9 mm). This would result in a fibre volume fraction of 60 % for C/LMPAEK adherends after consolidation versus 58 % for C/PEEK adherends. This increased fibre volume fraction can also account for the increase in storage modulus [51–53] and increase in loss modulus, since the energy dissipation via friction between matrix and fibres also increases with a larger amount of fibres in the C/LMPAEK adherends. The resulting values of the transverse storage modulus of the adherends are referred to as E'_{Ad} and are assumed to be constant.

For the sake of comparison, the viscoelastic heating rate is calculated at the temperature that presents the largest difference in the loss modulus between PEEK and LMPAEK EDs. That temperature corresponds to the measured T_g (156 °C) and it is also when the maximum viscoelastic heating rate occurs. Table 2 shows the values used to estimate the maximum viscoelastic heating rate at the energy director including the data obtained from the DMA experiments for the EDs (Fig. 8).

The temperature change of the ED due to the maximum viscoelastic heat, in an idealized adiabatic condition, can then be estimated according to:

$$d(\dot{Q}_{visc} t_{onset}) = d(m_{ED} c_{ED} T) \quad (3)$$

where \dot{Q}_{visc} is again the viscoelastic heating rate at the weld interface, t_{onset} is the time until onset of the flow, m_{ED} and c_{ED} are the mass and the specific heat capacity of the EDs being heated up, respectively, and T is the temperature change of the material. With a similar time until the onset of the flow, a possible explanation for the mostly similar temperature profiles for PEEK and LMPAEK welds in the parallel configuration relies on the heat capacity of LMPAEK being half of the heat capacity of PEEK at their respective T_m (see Fig. 9), which

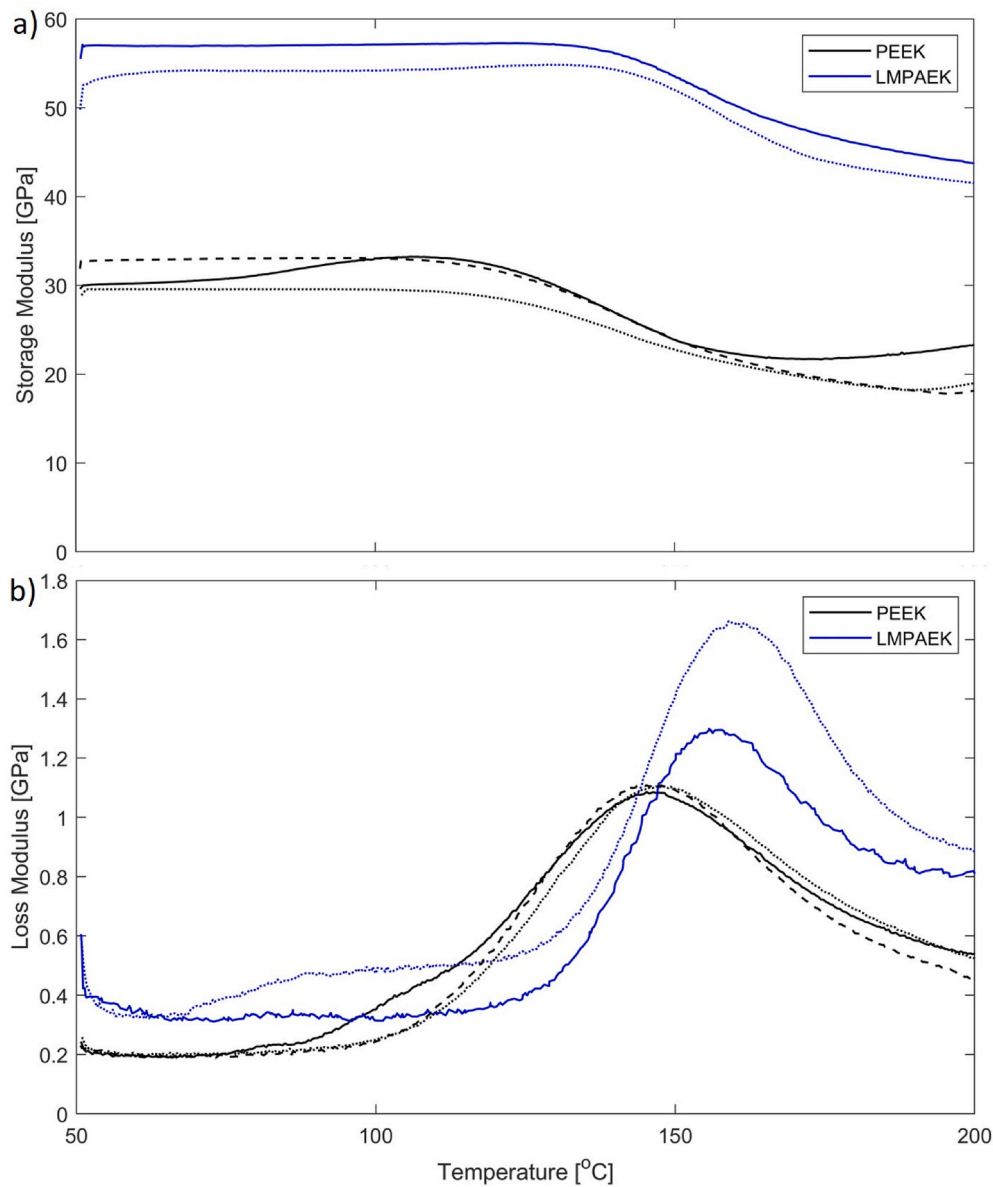


Fig. 10. Temperature dependency of a) Storage and b) Loss moduli of C/PEEK and C/LMPAEK adherends. Solid and dotted lines of same color indicate duplicate tests. (For interpretation of the references to colour in this figure legend, the reader is referred to the Web version of this article.)

Table 2

Parameters used to estimate the maximum viscoelastic heating rate for PEEK and LMPAEK welds on a parallel configuration.

	PEEK	LMPAEK	Source
Fibre volume fraction [%]	58	60	Datasheet [42] Calculated
L_{ED} [mm]	0.25	0.25	Measured
L_{Ad} [mm]	1.9	1.8	Measured
E'_{Ad} [GPa]	7.61	5.00	Calculated with Rule of Mixtures [50]
E'_{ED} at T_g [GPa]	0.97	0.88	From Fig. 8a
E''_{ED} at T_g [GPa]	0.226	0.144	From Fig. 8b
$\dot{Q}_{visc\ ED}$ [N/s.m ²]	5.31E+10	2.46E+10	Calculated from Equation 1

counterbalances the doubled viscoelastic heating rate of PEEK in comparison to LMPAEK welds (see Table 2).

The lower LMPAEK heat capacity in comparison to PEEK is believed to be a result of its lower degree of crystallinity, which was estimated via the melting enthalpy of each resin obtained from via mDSC. In literature, no enthalpy for 100 % crystalline LMPAEK has been reported so far, and to estimate the degree of crystallinity several authors have used the

enthalpy of 100 % crystalline PEEK, 130J/g, instead [54,55]. In case of the resin systems used in this study, using the 100 % enthalpy of PEEK, the crystallinity of PEEK ED would be estimated at 32 % and at 20 % for LMPAEK ED, which is in the range reported by other authors [40,56].

To verify the difference in crystallinity from a qualitative point of view, SEM images of the fracture surfaces of PEEK and LMPAEK parallel welds tested by SLS were made and are shown in Fig. 11. These welds

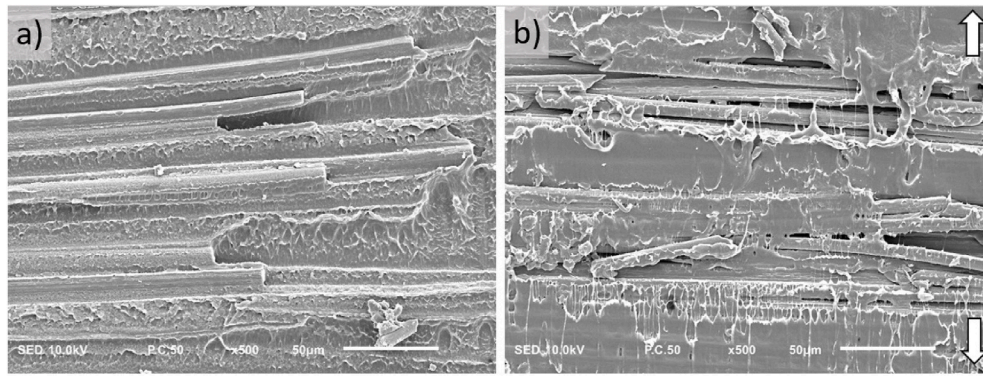


Fig. 11. SEM images of the fracture surface of a) PEEK and b) LMPAEK parallel welds. Both welds were stopped at the onset of the flow (displacement = 0.03 mm) and consolidation force of 500 N was applied for 4 s. White arrows indicate the direction of the load applied in shear for both welds. Magnification of 500x.

were stopped at the onset of the flow with consolidation pressure applied, which resulted in a still resin-rich fracture surface. The fracture surface of PEEK welds (Fig. 11a) shows that PEEK resin presents a more brittle behaviour, characterised by the little matrix deformation, in comparison to the plastic pattern observed in the fracture surface of LMPAEK welds. A brittle fracture, as the one observed for PEEK welds, has been associated with a higher degree of crystallinity [57], as it is the case for PEEK in comparison to LMPAEK.

For the parallel configuration, no significant difference in the resin colour across the adherends thickness could be observed in the cross-sectional micrographs, except at the layers at the vicinity of the weld interface, as indicated by the arrows in Fig. 4. This is due to the heat generation being focused at the weld interface (at least until the onset of the flow) for the parallel configuration. Therefore, only the layer closest to the weld interface is expected to reach T_m . This also is apparent as no porosity is observed at the layers farther from the weld interface for both PEEK and LMPAEK welds. The contribution of heat conduction to the through-thickness heating has been considered irrelevant based on the results presented by Jongbloed et al. [33]. In their work, the authors showed that heat conduction mainly takes place during the cooling phase, when ultrasonic vibration has already stopped.

While for the welds with parallel adherends, similar temperature profiles and similar times until the onset of the downward movement of the sonotrode were observed, that was not the case for the welds with misaligned adherends. For the latter ones, the downward movement of the sonotrode mainly occurs when the material at E2, the compressed edge, is molten [30]. Hence, the fact that LMPAEK welds reach their melting temperature at E2 earlier than PEEK welds (see Fig. 6) allows the downward movement of the sonotrode to also occur earlier. In misaligned welds, an angle of approximately 0.95° combined with a very short clamping distance (such as 5 mm as in our case) is already sufficient to result in most of the cyclic strain applied by the sonotrode to reach only the top adherend [30]. This shift from ED heating to bulk heating occurs because of the gap between top adherend and ED that is created by the misalignment angle. Consequently, the heat affected zone extends to the top adherend at much earlier stages of the ultrasonic welding process in comparison to parallel welds.

Due to the misalignment angle, we cannot model the welding stack adherend-ED-adherend as springs in series, as we have done previously for the parallel welds (Equation (2)). Instead, most of the amplitude of vibration is transmitted to the top adherend only [30], intensifying the bulk heating mechanism. Since both PEEK and LMPAEK welds have similar misalignment angles and are subjected to the same amplitude of vibration ($43.1 \mu\text{m}$), the cyclic strain on the top adherend, ϵ_{Ad} , is simply given by:

$$\epsilon_{Ad} = \frac{\Delta L}{L_{Ad}} \quad (4)$$

Table 3

Parameters used to estimate the maximum bulk viscoelastic heating rate for C/PEEK and C/LMPAEK adherends in misaligned welds.

	PEEK	LMPAEK	Source
ϵ_{Ad} [–]	0.0227	0.0239	Calculated from Equation 4
E''_{Ad} at T_g [GPa]	1.10	1.47	From Fig. 10b
Q_{viscAd} [N/s.m ²]	3.55E+10	5.29E+10	Calculated from Equation 1

where ΔL is the amplitude of vibration and L_{Ad} is the thickness of the adherend. The calculated cyclic strain on the top adherend can then be used to estimate the maximum bulk viscoelastic heating rate generated in the top adherend. For this, Equation (1) is again used, but with the subscript Ad replacing the subscript ED to indicate that the properties of the composite material are being used instead of the resin ones. The maximum loss modulus of the adherend is obtained via the DMA results showed in Fig. 10b. The parameters used to estimate the maximum bulk viscoelastic heating rate on the top adherend are summarized in Table 3.

We can see that for misaligned welds, our calculations indicate that the C/LMPAEK adherend presents a bulk heating rate 1.5 times higher than the one for C/PEEK adherend. This, in combination with the higher heat capacity of C/PEEK adherend, would result in a rate of change in temperature higher for C/LMPAEK adherends. As we have mentioned before, the heat capacity is affected by the degree of crystallinity of the material. Although the degree of crystallinity of the resin in the adherends may differ from the degree of crystallinity of the pure resin [58], the degree of crystallinity of C/LMPAEK is anyways expected to remain lower than the one for C/PEEK due to its higher fibre volume fraction (60 % for C/LMPAEK versus 58 % for C/PEEK), which reduces the space between fibres, limiting the growth of the crystalline phase [57]. To quantify the rate of change in temperature for the adherends, we assume that the ratio between C/PEEK and C/LMPAEK heat capacities remains of about 2 times, like the ratio between the heat capacities of PEEK and LMPAEK resins. This would result in a rate of change in temperature almost 3 times higher for C/LMPAEK adherend than for C/PEEK adherends. The estimated higher bulk heating rate and consequent faster temperature increase in C/LMPAEK adherends is corroborated by the overall higher temperature profile of LMPAEK welds (see Fig. 6) and its 1.7 times higher rate of change in temperature in comparison to PEEK welds in the misaligned configuration. Such a higher estimated rate of change in temperature ratio between LMPAEK and PEEK welds in comparison to the experimental one (3 times versus 1.7 times, respectively) is believed to derive from the simplifications done in our calculations, in addition to neglecting the role of process efficiency and hammering coefficient in the process. The process efficiency would account for the several losses that occur during the process, such as acoustic losses, dissipation in the composite adherends and in the rig and the efficiency of the equipment itself [29], while the hammering

coefficient considers the loss of contact between the sonotrode and the top adherend that occurs during the vibration phase [59].

The higher temperature change in LMPAEEK welds is also in agreement with what is observed in the cross-sectional micrographs shown in Fig. 7, as they indicate that the C/LMPAEEK adherends are more affected by bulk heating than the C/PEEK adherends. This interpretation of the cross-sectional micrographs is based on two observations: 1) the appearance of the resin throughout the thickness of the adherends and 2) the larger squeeze flow observed in C/LMPAEEK welds. For observation (1), the white/light grey colour of the resin-rich areas that are present throughout the misaligned C/PEEK adherends (indicated by the black arrows in Fig. 7) is indicative of a semi-crystalline state. Contrarily, the dark grey tone observed in the resin-rich areas that are more present in C/LMPAEEK adherends (indicated by the red arrows in Fig. 7) is characteristic of an amorphous state [60]. Hence, this difference in colour indicates that melting and fast cooling occurred in most of the C/LMPAEEK bulk adherends during the welding process of misaligned adherends, which resulted in the more predominant amorphous state of the cooled LMPAEEK resin. Regarding observation (2), the larger squeeze flow of the molten resin from the C/LMPAEEK adherends is evidenced by the shorter inter-ply distance in the free edge of the top adherend (Edge 1) and the ply distortion in the bottom adherend (see Fig. 7), which is not observed in the C/PEEK adherends. In addition to this, we also observed that LMPAEEK welds always presented a larger travel distance in comparison to PEEK welds. This travel distance corresponds to the entire distance travelled by the sonotrode during the ultrasonic welding process, also taking into account the distance travelled during the consolidation phase, when any molten material continues to be squeezed out until the whole welding stack is again under T_m . For the parallel case, full welds resulted in a travel distance of 0.46 mm for PEEK welds and 0.47 mm for LMPAEEK welds. For the misaligned case stopped at the onset of the downward movement of the sonotrode, the travel distance was 0.11 mm on average for PEEK welds and 0.14 mm on average for LMPAEEK welds. These values reinforce the overall larger squeeze flow observed for LMPAEEK welds, irrespective of the configuration used, in comparison to PEEK welds.

5. Conclusions

Our objective with this paper was to investigate how the resin used as matrix in the adherends and in the energy director affects the ultrasonic welding process of welds in both parallel and misaligned configurations. The main take-aways of this work are.

- In a parallel configuration, changing the resin did not result in significant differences on power or sonotrode displacement, temperature profiles or through-thickness heating. Estimating the viscoelastic heating rate and temperature change at the weld interface showed that such similarities come from the counter-balance between a higher viscoelastic heating rate (mainly affected by the magnitude of the loss modulus peak) and a lower heat capacity of the LMPAEEK resin in comparison to PEEK. The through-thickness heating of adherends is not expected to significantly differ despite of the resin used since heat generation is concentrated at the weld interface for parallel welds.
- In a misaligned configuration, a shorter duration of the process was observed for LMPAEEK welds, as well as a faster temperature increase and C/LMPAEEK adherends being more affected by through-thickness heating in comparison to C/PEEK. These differences observed for misaligned welds derive from the bulk heating being the protagonist in this configuration, in contrast to what happens in the parallel configuration, where heat generation is mainly focused at the weld interface. The higher loss modulus peak of the C/LMPAEEK adherend resulted in a higher bulk heating which, combined with a lower heat capacity of LMPAEEK, lead to a higher rate of change in temperature and overall temperature profile.

- In general terms, the viscoelastic heating rate at the weld interface, which is in turn mainly governed by the magnitude of the loss modulus peak of the ED, and the heat capacity of the resin are the two principal parameters to look at when comparing the behaviour of different resins used to weld parallel adherends. On the other hand, the bulk heating rate, which is in turn mainly governed by the magnitude of the loss modulus peak of the top adherend, and again the heat capacity of the resin are the two principal parameters to compare the behaviour of different resins used to weld misaligned adherends.
- Other parameters also have relevance when changing the resin used to manufacture the ED and the adherends used in ultrasonic welding. The degree of crystallinity of the resin affects the process in both parallel and misaligned configurations, since it influences the resin heat capacity. The fibre volume fraction of the laminate will also play a significant role when welding misaligned adherends, since it influences the loss modulus of the top adherend and consequently the bulk heating rate during the welding process.

CRediT authorship contribution statement

C.B.G. Brito: Writing – original draft, Visualization, Methodology, Investigation, Formal analysis, Conceptualization. **J. Teuwen:** Writing – review & editing, Supervision, Conceptualization. **C.A. Dransfeld:** Writing – review & editing, Supervision, Resources. **I.F. Villegas:** Writing – original draft, Supervision, Funding acquisition, Data curation, Conceptualization.

Declaration of competing interest

The authors declare that they have no known competing financial interests or personal relationships that could have appeared to influence the work reported in this paper.

Acknowledgements

We would like to thank the Faculty of Mechanical, Maritime and Materials Engineering of TU Delft for allowing the use of their SEM equipment for the analysis carried out in this work.

The work presented in this paper is carried out as part of a project, which has received funding from the Clean Sky 2 Joint Undertaking (JU) under the European Union's Horizon 2020 research and innovation programme under grant agreement No 776455. The results, opinions, conclusions, etc. presented in this work are those of the author(s) only and do not necessarily represent the position of the JU; the JU is not responsible for any use made of the information contained herein.

Data availability

The raw/processed data required to reproduce these findings cannot be shared at this time as the data also forms part of an ongoing study.

References

- [1] Bhudolia S, Gohel G, Leong K, Islam A. Advances in ultrasonic welding of thermoplastic composites: a review. *Mater* 2020;13(1284).
- [2] Costa A, Botelho E, Costa M, Narita N, Tarpani J. A review of welding technologies for thermoplastic composites in aerospace applications. *J Aerosp Technol Manag* 2012;4(3):255–65.
- [3] Diaz J, Rubio L. Developments to manufacture structural aeronautical parts in carbon fibre reinforced thermoplastic materials. *J Mater Process Technol* 2003; 143–144:342–346.
- [4] Offringa A. Thermoplastic composites—rapid processing applications. *Compos Appl Sci Manuf* 1996;27(4).
- [5] Vincent G, de Bruijn T, Wijskamp S, Rasheed M, van Dongen M, Akkerman R. Characterisation and improvement of the quality of mixing of recycled thermoplastic composites. *Compos C* 2021;4:100108.

- [6] Vincent G, de Bruijn T, Wijskamp S, Rasheed M, van Drongelen M, Akkerman R. Shredding and sieving thermoplastic composite scrap: method development and analyses of the fibre length distributions. *Compos B Eng* 2019;176:107197.
- [7] Ageorges C, Yea L, Hou M. Advances in fusion bonding techniques for joining thermoplastic matrix composites: a review. *Compos Appl Sci Manuf* 2001;32: 839–57.
- [8] Guo Q. *Thermosets: structure, properties and applications*. Cambridge, UK: Woodhead Publishing; 2012.
- [9] Barile M, Lecce L, Iannone M, Pappadà S, Roberti P. Thermoplastic composites for aerospace applications. In: Pantelakis S, Tserpes K, editors. *Revolutionizing aircraft materials and processes*. Springer; 2020.
- [10] Falzon B, Pierce R. Thermosetting composite materials in aerostructures. In: Pantelakis S, Tserpes K, editors. *Revolutionizing aircraft materials and processes*. Springer; 2020.
- [11] A. Yousefpour, M. Hojjati and J. Immarigeon, "Fusion bonding/welding of thermoplastic composites," *J Thermoplast Compos Mater*, vol. 17, pp. 303-340.
- [12] Taylor N, Jones S, Weld M. The feasibility of welding thermoplastic composite materials. *Constr Build Mater* 1989;3(4):213–9.
- [13] Ozturk F, Cobanoglu M, Ece R. Recent advancements in thermoplastic composite materials in aerospace industry. *J Therm Compos Mater* 2023;1–33.
- [14] Gonçalves L, Duarte F, Martins C, Paiva M. Laser welding of thermoplastics: an overview on lasers, materials, processes and quality. *Infrared Phys Technol* 2021; 119.
- [15] Iftikhar S, Mourad A-H, Sheikh-Ahmad J, Almaskari F, Vincent S. A comprehensive review on optimal welding conditions for friction stir welding of thermoplastic polymers and their composites. *Polym* 2021;13.
- [16] Kumar R, Singh R, Ahuja I, Penna R, Feo L. Weldability of thermoplastic materials for friction stir welding- A state of art review and future applications. *Compos B Eng* 2018;137:1–15.
- [17] Villegas I, Moser L, Yousefpour A, Mitschang P, Bersee H. Process and performance evaluation of ultrasonic, induction and resistance welding of advanced thermoplastic composites. *J Thermoplast Compos Mater* 2013;26(8):1007–24.
- [18] Larsen L, Endrass M, Jarka S, Bauer S, Janek M. Exploring ultrasonic and resistance welding for thermoplastic composite structures: process development and application potential. *Compos B Eng* 2025;289.
- [19] Reis J, de Moura M, Samborski S. Thermoplastic composites and their promising applications in joining and repair composite structures: a review. *Mater* 2020;13.
- [20] Stavrov D, Bersee H. Resistance welding of thermoplastic composites-an overview. *Compos Appl Sci Manuf* 2005;36:39–54.
- [21] Bayerl T, Duhovic M, Mitschang P, Bhattacharyya D. The heating of polymer composites by electromagnetic induction – a review. *Compos Appl Sci Manuf* 2014; 57:27–40.
- [22] Ahmed T, Stavrov D, Bersee H, Beukers A. Induction welding of thermoplastic composites—an overview. *Compos Appl Sci Manuf* 2006;37(10):1638–51.
- [23] Grewell D, Benatar A. Welding of plastics: fundamentals and new developments. *Int Polym Process* 2007;22(1):43–60.
- [24] Villegas I. In situ monitoring of ultrasonic welding of thermoplastic composites through power and displacement data. *J Thermoplast Compos Mater* 2015;28(1): 66–85.
- [25] Tsiangou E, Teixeira de Freitas S, Villegas IF, Benedictus R. Ultrasonic welding of epoxy-to polyetheretherketone-based composites: Investigation on the material of the energy director and the thickness of the coupling layer. *J Compos Mater* 2020: 1–18.
- [26] Benatar A, Gutowski T. Ultrasonic welding of PEEK graphite APC-2 composites. *Polym Eng Sci* 1989;29.
- [27] Zhang Z, Wang X, Luo Y, Zhang Z, Wang L. Study on heating process of ultrasonic welding of thermoplastics. *J Thermoplast Compos Mater* 2021;23:647–64.
- [28] Palardy G, Shia H, Levy A, Le Corre S, Villega I. A study on amplitude transmission in ultrasonic welding of thermoplastic composites. *Compos Appl Sci Manuf* 2018; 113:339–49.
- [29] Levy A, Le Corre S, Villegas I. Modeling of the heating phenomena in ultrasonic welding of thermoplastic composites with flat energy directors. *J Mater Process Technol* 2014;214:1361–71.
- [30] Brito C, Teuwen J, Dransfeld C, Villegas I. The effects of misaligned adherends on static ultrasonic welding of thermoplastic composites. *Compos Appl Sci Manuf* 2022;155:106810.
- [31] Brito C, Teuwen J, Dransfeld C, Villegas I. On improving process efficiency and weld quality in ultrasonic welding of misaligned thermoplastic composite adherends. *Compos Struct* 2023;304(2).
- [32] Jongbloed B, Teuwen J, Benedictus R, Villegas I. On differences and similarities between static and continuous ultrasonic welding of thermoplastic composites. *Compos B Eng* 2020;203.
- [33] Jongbloed B, Teuwen J, Benedictus R, Villegas I. A study on through-the-thickness heating in continuous ultrasonic welding of thermoplastic composites. *Mater* 2021; 14(6620).
- [34] Jongbloed B, Vinod R, Teuwen J, Benedictus R, Villegas I. Improving the quality of continuous ultrasonically welded thermoplastic composite joints by adding a consolidator to the welding setup. *Compos - A: Appl Sci Manuf* 2022;155.
- [35] E. Kuram, "Hybrid biocomposites: utilization in aerospace engineering," in *Advanced composites in aerospace engineering applications*, Springer.
- [36] Wang X, Xu J, Chen S, Li Y, Gao G, Gu W, Sha M. Damage behavior and assessment of aeronautical PMMA subjected to high-velocity water-jet impact. *Wear* 2023: 534–5.
- [37] Beukers A, Bersee H, Koussios S. *Future aircraft structures: from metal to composite structures*. In: Nicolas L, Meo M, Milella E, editors. *Composite materials - a vision for the future*. London: Springer; 2011.
- [38] Seki Y, Kizilkan E, Leşkeri BM, Sarikanat M, Altay L, Isbilir A. Comparison of the thermal and mechanical properties of poly(phenylene sulfide) and poly(phenylene sulfide)-syndiotactic polystyrene-based thermal conductive composites. *ACS Omega* 2022;7(49):45518–26.
- [39] Bonmatin M, Chabert F, Bernhart G, Djilali T. Rheological and crystallization behaviors of low processing temperature poly(aryl ether ketone). *J Appl Polym Sci* 2021;138(47).
- [40] Audoit J, Rivière L, Dandurand J, Lonjon A, Dantras E, Lacabanne C. Thermal, mechanical and dielectric behaviour of poly(aryl ether ketone) with low melting temperature. *J Therm Anal Calorim* 2019;134(4):2147–57.
- [41] Jongbloed B, Teuwen J, Palardy G, Villegas I, Benedictus R. Continuous ultrasonic welding of thermoplastic composites: enhancing the weld uniformity by changing the energy director. *J Compos Mater* 2019;1–13.
- [42] Composites TA. *Toray Cetex® TC1200 PEEK - product data sheet [Online]*. Available: https://www.toraytac.com/media/7765d981-1f9f-472d-bf24-69a647412e38/Pr7gdw/TAC/Documents/Data_sheets/Thermoplastic/UD%20tapes,%20prepregs%20and%20laminates/Toray-Cetex-TC1200_PEEK_PDS.pdf. [Accessed 15 September 2023].
- [43] Composites TA. *Toray Cetex® TC1225 LMPAEEK - product data sheet [Online]*. Available: https://www.toraytac.com/media/3bd72fac-0406-48e4-bfc4-2ffd2398ac0c/zipxA/TAC/Documents/Data_sheets/Thermoplastic/UDtapes%20Cprepregsandlaminates/Toray-Cetex-TC1225_PAEK_PDS.pdf. [Accessed 15 September 2023].
- [44] Villegas I. Strength development versus process data in ultrasonic welding of thermoplastic composites with flat energy directors and its application to the definition of optimum processing parameters. *Compos Appl Sci Manuf* 2014;27–37.
- [45] Villegas I, Grande B, Bersee H, Benedictus R. A comparative evaluation between flat and traditional energy directors for ultrasonic welding of CF/PPS thermoplastic composites. *Compos Interfaces* 2015;22:1–13.
- [46] Palardy G, Villegas I. On the effect of flat energy directors thickness on heat generation during ultrasonic welding of thermoplastic composites. *Compos Interfaces* 2017;24:203–14.
- [47] Liu J, Yue D, Wang X, Pan J, Yang D, Quan D, Zhao G. Effects of welding displacement and energy director thickness on the ultrasonic welding of epoxy-to-polyetherimide based hybrid composite joints. *Compos Sci Tech* 2024;257.
- [48] Köhler F, F VI, Dransfeld C, Herrmann A. Static ultrasonic welding of carbon fibre unidirectional thermoplastic materials and the influence of heat generation and heat transfer. *J Compos Mater* 2021;55(15):2087–102.
- [49] Tateishi N, North T, Woodhams R. Ultrasonic welding using tie-layer materials. Part I: analysis of process operation. *Polym Eng Sci* 1992;32:600–11.
- [50] Jacquet E, Trivaudey F, Varchon D. Calculation of the transverse modulus of a unidirectional composite material and of the modulus of an aggregate. Application of the rule of mixtures. *Compos Sci Technol* 2000;60(3):345–50.
- [51] Pothan LA, Thomas S, Groeninckx G. The role of fibre/matrix interactions on the dynamic mechanical properties of chemically modified banana fibre/polyester composites. *Compos Appl Sci Manuf* 2006;37:1260–9.
- [52] Qiao J, Zhang Q, Wu C, Wu G, Li L. Effects of fiber volume fraction and length on the mechanical properties of milled glass fiber/polyurea composites. *Polymers* 2022;14(15):3080.
- [53] Asim M, Jawaid M, Nasir M, Saba N. Effect of fiber loadings and treatment on dynamic mechanical, thermal and flammability properties of pineapple leaf fiber and kenaf phenolic composites. *J. Renew. Mater.* 2018;6(4).
- [54] Yap T, Heathman N, Phillips T, Beaman J, Tehrani M. Additive Manufacturing of Polyaryletherketone (PAEK) polymers and their composites. *Compos B Eng* 2023; 266.
- [55] Blundell D, Osborn B. The morphology of poly(aryl-ether-etherketone). *Polym* 1983;24.
- [56] Gao S-L, Kim J-K. Cooling rate influences in carbon fibre/PEEK composites. Part 1. Crystallinity and interface adhesion. *Compos Appl Sci Manuf* 2000;31:517–30.
- [57] Perez-Martín H, Mackenzie P, Baidak A, Bradaigh CMO, Ray D. Crystallinity studies of PEKK and carbon fibre/PEKK composites: a review. *Compos B Eng* 2021; 223:109127.
- [58] Heathman N, Koirala P, Yap T, Emami A, Tehrani M. In situ consolidation of carbon fiber PAEK via laser-assisted automated fiber placement. *Compos B Eng* 2023;249.
- [59] Nonhof C, Luiten G. Estimates for process conditions during the ultrasonic welding of thermoplastics. *Polym Eng Sci* 1996;36(9):1177–83.
- [60] Koutras N, Amirdine J, Boyard N, Villegas I, Benedictus R. Characterisation of crystallinity at the interface of ultrasonically welded carbon fibre PPS joints. *Compos Appl Sci Manuf* 2019;125:105574.